TU Delft

Delft University of Technology

A multicomponent pseudopotential lattice Boltzmann model for liquid–liquid systems with soluble surfactants

Pourtousi, Mohammad; Safdari, Arman; Shardt, Orest; Van den Akker, Harry E.A.

DOI
10.1016/j.ijmultiphaseflow.2025.105255

Publication date
2025

Document Version
Final published version

Published in
International Journal of Multiphase Flow

Citation (APA)
Pourtousi, M., Safdari, A., Shardt, O., & Van den Akker, H. E. A. (2025). A multicomponent pseudopotential lattice Boltzmann model for liquid–liquid systems with soluble surfactants. *International Journal of Multiphase Flow*, *189*, Article 105255. https://doi.org/10.1016/j.ijmultiphaseflow.2025.105255

Important note
To cite this publication, please use the final published version (if applicable).
Please check the document version above.

Copyright
Other than for strictly personal use, it is not permitted to download, forward or distribute the text or part of it, without the consent of the author(s) and/or copyright holder(s), unless the work is under an open content license such as Creative Commons.

Takedown policy
Please contact us and provide details if you believe this document breaches copyrights.
We will remove access to the work immediately and investigate your claim.

This work is downloaded from Delft University of Technology.
For technical reasons the number of authors shown on this cover page is limited to a maximum of 10.

International Journal of Multiphase Flow 189 (2025) 105255

Contents lists available at ScienceDirect

International Journal of Multiphase Flow

journal homepage: www.elsevier.com/locate/ijmulflow

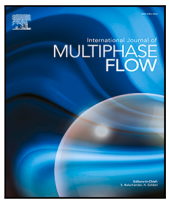

A multicomponent pseudopotential lattice Boltzmann model for liquid–liquid systems with soluble surfactants

Mohammad Pourtousi [a,b,1], Arman Safdari [a,b,1], Orest Shardt [a,b,d], Harry E.A. Van den Akker [a,b,e,c,*]

[a] SSPC, Taighde Éireann – Research Ireland Centre for Pharmaceuticals, University of Limerick, Limerick, V94 T9PX, Ireland
[b] Bernal Institute, University of Limerick, Castletroy, Limerick, V94 T9PX, Ireland
[c] Delft University of Technology, Department of Chemical Engineering, Van der Maasweg 9, Delft, 2629 HZ, The Netherlands
[d] Department of Chemical Sciences, University of Limerick, Castletroy, Limerick, V94 T9PX, Ireland
[e] School of Engineering, University of Limerick, Castletroy, Limerick, V94 T9PX, Ireland

ARTICLE INFO

Keywords:
liquid–liquid dispersions
Lattice Boltzmann
Multicomponent pseudopotential
Surfactant behaviour
Shear
Droplet deformation and breakup

ABSTRACT

The intermolecular interactions in the pseudo-potential lattice Boltzmann (PPLB) method can readily be extended to more than two components. We report about a three-component PPLB approach to explore whether the effect of a surfactant could be included in describing droplet behaviour in (liquid–liquid) emulsions. The two main liquid components are taken to follow the Carnahan-Starling equation of state (EoS), while the surfactant obeys an ideal EoS. We investigate the nature of the phases present at equilibrium and the dependence of the interfacial tension between the two liquid phases on the amount of surfactant. The response of a droplet subjected to simple shear is investigated in the absence and the presence of a surfactant. Our exploratory simulations show how during droplet deformation the surfactant re-distributes itself due to the action of the shear and flows towards the far ends of the deformed droplet, up to the moment the droplet breaks up. This inhomogeneous surfactant distribution along the interface increases the shear rate that is needed for droplet breakup such that the critical capillary number for breakup increases and the breakup process is delayed. The simulations also reveal the detailed flow fields inside and outside the deforming droplet.

1. Introduction

Many computational fluid dynamics (CFD) methods are available to simulate multicomponent, multiphase flows for industrial applications such as emulsification. First, there is a variety of interface capturing algorithms, such as level set (LS) and volume of fluid (VOF), which can be coupled with solvers for the Navier–Stokes equations (usually exploiting finite volume methods) to compute multiphase flows. While these computational approaches can describe the evolution of the interfaces that separate fluid phases, they do not consider and model the underpinning intermolecular interactions that lead to phase separation. As such, they do not contribute much to the understanding of the physico-chemical details of interfacial phenomena including the behaviour of a surfactant which is the topic of this paper.

Over the past few decades, lattice Boltzmann (LB) techniques have been increasingly applied to simulate all types of multiphase flows. Since these techniques are based on a kinetic equation for particle distribution functions, they are considered mesoscopic-scale simulation methods that occupy a middle ground between molecular dynamics simulations and methods that consider only macroscopic fluid scales (Chen et al., 2014; Zarghami et al., 2015; Van den Akker, 2018). The local nature of the calculations in LB enables efficient parallelization and therefore faster computations (Krüger et al., 2017). A drawback of LB methods is that, depending on the lattice (grid) density, phase interfaces become diffuse, i.e. the composition of an interface varies smoothly across the interface (Engblom et al., 2013; Mukherjee et al., 2019a).

A popular class of LB models is based on a phase-field model for simulating the interface position and behaviour by exploiting a free energy function (Cahn-Hilliard or Landau-Ginzburg). The phase field equation is then combined with a Navier–Stokes equation to include the flow and interface dynamics. Any phase field model consists of a series of complex equations with several empirical parameters which can be used to tune the physics and to stabilize the numerical solution. Further details can be found in e.g. Kian Far et al. (2023).

* Corresponding author at: Bernal Institute, University of Limerick, Castletroy, Limerick, V94 T9PX, Ireland.
E-mail address: Harry.VanDenAkker@ul.ie (H.E.A. Van den Akker).
[1] Authors contributed equally.

https://doi.org/10.1016/j.ijmultiphaseflow.2025.105255
Received 29 November 2024; Received in revised form 4 April 2025; Accepted 7 April 2025
Available online 21 April 2025
0301-9322/© 2025 The Authors. Published by Elsevier Ltd. This is an open access article under the CC BY license (http://creativecommons.org/licenses/by/4.0/).

In the Pseudo-Potential lattice Boltzmann (PPLB) method, also called the Shan–Chen model (Shan and Chen, 1993; Shan and Doolen, 1995), the thermodynamic behaviour is described by an inter-particle potential; through the choice of this potential, the simulated fluid can obey arbitrary equations of state (EOSs). Separation of a multicomponent mixture into different phases can be modelled via a single short-range force between the components that models molecular attraction or repulsion between components. In comparison with conventional CFD models, the formation and evolution of phase interfaces are captured automatically in PPLB, as molecular interactions are incorporated as the driving force for phase separation. In addition, unlike mesh-based methods, the PPLB approach allows a straightforward treatment of topological changes, i.e. merging and splitting of interfaces. As a result, the PPLB approach may be closer to physics and is mathematically simpler. Drawbacks of PPLB are that surface tension is just the result of a simulation (such that iterations are required to mimic a real-life two-phase flow system with a targeted surface tension) and that PPLB simulations are more sensitive to numerical instabilities, with fewer options for tuning. Many successful two-phase flow simulations with PPLB have been reported in the literature, such as (Kamali and Van Den Akker, 2013; Zarghami et al., 2015; Huang et al., 2007; Chen et al., 2014; Mukherjee et al., 2019a,b; Van den Akker, 2018).

This paper then focuses on the role of a surfactant in emulsions. By accumulating along interfaces, surfactants affect droplets in many ways, including their shape when subjected to shear, the velocity distributions within them, and the conditions under which they break up (and coalescence).

Studies of these phenomena have been reported for different numerical methods such as phase field (Soligo et al., 2019), smoothed particle hydrodynamics (SPH) (Adami et al., 2010), front tracking (de Jesus et al., 2015), level set (Xu et al., 2006), and free energy LBM (Komrakova et al., 2014; Van Der Sman and Meinders, 2016). These methods were found to be capable of modelling the effects of surfactant concentration on the interfacial tension between phases and on droplet dynamics (de Jesus et al., 2015; Lee and Pozrikidis, 2006; Pan et al., 2016). This paper now reports about our study as to whether the simpler and faster PPLB method can (also) be used to elucidate the impact of a surfactant in emulsions. Earlier, we reported how to include a surfactant as the third component in PPLB simulations and applied the method to drop formation from an aperture (Mukherjee et al., 2019a). In this paper, we report about the role of a surfactant in the deformation and breakup of a single droplet in a simple shear flow.

During shear-driven droplet deformation, the shear may also induce a non-uniform distribution of a surfactant across the interface which may result in tangential Marangoni stresses in the direction from high to low surfactant concentration (i.e., from low to high interfacial tension). Such Marangoni stresses balance the shear stresses exerted on the droplet to effect a different droplet shape than without a surfactant. Modelling these stresses is therefore essential for simulations of surfactant-laden droplets and other interfacial flows with spatially varying interfacial tension (Sui, 2014; Liu et al., 2018).

The effects of non-uniform surfactant concentrations on droplet deformation and break-up in shear flow have been observed in many papers. Several authors (Liu and Zhang, 2010; Engblom et al., 2013; Van Der Sman and Meinders, 2016; Shi et al., 2019; Soligo et al., 2019; Kian Far et al., 2023; Chen et al., 2023; Zhou et al., 2023; Zhang et al., 2024) improved and applied phase-field LB methods for investigating the role and impact of mainly soluble surfactants. A detailed review of their methods and findings is beyond the scope of this paper. Soligo et al. (2019) modelled the effects of a surfactant on interfacial tension through an EOS and showed that the presence of a surfactant increases deformability by shear. Van der Sman and Van der Graaf (2006) found that during deformation of a droplet the surfactant accumulated at the regions of the droplet interface with the highest curvature. Liu and Zhang (2010) and Shi et al. (2019) reported that increasing amounts of surfactant result in increasing deformation of a droplet (expressed in terms of the Taylor deformation parameter D), faster droplet breakup, and production of more droplets compared to clean (i.e., surfactant-free) liquid–liquid dispersions (Shi et al., 2019). Similar findings have been reported by Chen et al. (2023), Zhou et al. (2023) and Zhang et al. (2024).

Liu et al. (2018) used a hybrid lattice Boltzmann–finite difference method to model droplets with an insoluble surfactant. For low confinement ratios (ratio of droplet size to the distance between the sheared walls) the presence of surfactants delays droplet break-up. With high confinement ratios, the presence of surfactants promotes breakup. Shang et al. (2023) used a front-tracking method for simulating interfacial flows with particles and soluble surfactants with a focus on droplet dynamics, deformation and agglomeration.

As said, we explored the applicability of a three-component PPLB to shear-driven droplet deformation and breakup. Few PPLB simulations with more than two components have been reported in the literature. In simulations of Janus droplets (Shardt et al., 2014), which are pairs of adhering droplets of different fluids that are suspended in a third fluid, all three components were present in comparable amounts. In the present work, the amount of one component (the surfactant) is present in a much lower quantity than the other two. This is also the case in recent work, which we now extend, by Mukherjee et al. (2019a), who used PPLB to simulate a liquid–liquid dispersion with a soluble surfactant. To include the inter-component interaction force, they used the original Shan–Chen method (Shan and Chen, 1993). In 3D simulations of spinodal decomposition with a surfactant, they found that inclusion of a surfactant component changes the droplet size distribution and the dynamics of newly-formed droplets.

In this paper, we present a PPLB surfactant model in which the two liquid phases are described by a Carnahan-Starling equation of state. The surfactant component, which is present in small concentrations relative to those of the primary liquid phases, is modelled with an ideal equation of state. All three components interact with each other through repulsive forces. We show how the surfactant concentration accumulates at the interfaces between the liquid phases due to the action of the mutual G-values and affects the breakup of droplets. In the presence of shear, our PPLB method spontaneously leads to a non-uniform spatial distribution of the surfactant along interfaces. We observe that in the presence of such non-uniform surfactant concentrations a higher shear rate is needed to break up a droplet — an effect attributed to Marangoni stress.

All simulations reported in this paper are in 2-D. While nothing restricts us from running 3-D simulations, which do require substantial more computational time, there is no need to go beyond 2-D to demonstrate that a PPLB surfactant model works and delivers appealing and qualitatively correct results. In Section 2, we now will first detail all our PPLB model equations.

2. Methods

2.1. Lattice Boltzmann method

In LBM, the movement of fluids at macroscopic scales is related to the evolution of particle distributions in a discrete lattice (Chen and Doolen, 1998; Krüger et al., 2017; Van den Akker, 2018). Mimicking the behaviour of gas molecules, the fictitious LB particles move (stream) between lattice sites and collide, which is modelled as relaxation to an equilibrium distribution. In the absence of forces, the standard LB equation with the Bhatnagar-Gross-Krook (BGK) collision operator is

$$f_i^{\sigma}(\vec{x}+c\vec{e}_i\Delta t, t+\Delta t) - f_i^{\sigma}(\vec{x},t) = -\frac{\Delta t}{\tau^{\sigma}}\left(f_i^{\sigma}(\vec{x},t) - f_i^{\sigma,eq}(\vec{x},t)\right), \quad (1)$$

where the left side describes streaming and the right side describes relaxation to equilibrium. Since we consider a multicomponent system, the equation has been written for an arbitrary component σ. Each

component occupies its own lattice and has its own populations $f_i^\sigma(\vec{x},t)$ at every position $\vec{x}$ in the lattice and time t. The subscript i counts over the discrete directions of the lattice. The lattice speed is $c = \Delta x/\Delta t$, and we take $\Delta x = \Delta t = 1$. Note that in LB all variables are in LB units, i.e. are reported without units. τ^σ is the relaxation time, which determines the kinematic viscosity of each component. All simulations we present use a D2Q9 lattice, which has nine directions $\vec{e}_i$ ($i = 0, 1, \ldots, 8$) in two dimensions, and the isothermal speed of sound c_s is given by $c_s^2 = RT = 1/3$, with RT being the product of the gas constant and the absolute system temperature. The equilibrium distribution $f_i^{\sigma,eq}$ is a function of the local density ρ^σ and fluid velocity $\vec{u}^\sigma$ according to

$$f_i^{\sigma,eq} = w_i \rho^\sigma \left[1 + \frac{\vec{e}_i \cdot \vec{u}^\sigma}{RT} + \frac{(\vec{e}_i \cdot \vec{u}^\sigma)^2}{2(RT)^2} - \frac{\vec{u}^\sigma \cdot \vec{u}^\sigma}{2RT}\right], \tag{2}$$

where the weight factors are $w_0 = 4/9$, $w_{1-4} = 1/9$ and $w_{5-8} = 1/36$. ρ^σ and $\vec{u}^\sigma$ are computed as the zeroth and first moments of f_i^σ:

$$\rho^\sigma = \sum_i f_i^\sigma, \quad \rho^\sigma \vec{u}^\sigma = \sum_i \vec{e}_i f_i^\sigma. \tag{3}$$

At the macroscopic level, the LBM equations solve the continuity and Navier–Stokes equations for weakly compressible flow (Krüger et al., 2017). Pressure follows from the equation of state $P^\sigma = \rho^\sigma RT$, and the viscosity ν^σ of a component is $\nu^\sigma = c_s^2(\tau^\sigma - 1/2)$.

As presented thus far, the LB scheme would describe the flow of a single ideal component in the absence of body forces. The sections that follow describe the modifications of this basic LB scheme that are needed to: (a) specify a non-ideal equation of state for each component (or at least the two main components) and (b) introduce coupling between the components, including repulsive interactions that induce phase separation. These effects were incorporated into our LB model by adding to the right-hand side of a source term S_i that acts as a vehicle for the forces involved.

2.2. Multicomponent, multiphase pseudo-potential model

Rather than using the ideal LB EOS $P^\sigma = c_s^2\rho^\sigma$, we allow for arbitrary EOSs, by introducing for each component σ a self-interaction (or intra-molecular) force $\vec{F}^\sigma$ in terms of an effective mass or pseudo-potential ψ

$$\vec{F}^\sigma = \psi^\sigma(\vec{x}) \sum_i w_i \psi^\sigma(\vec{x} + \vec{e}_i)\vec{e}_i \tag{4}$$

in which

$$\psi = \sqrt{\frac{2}{c_s^2}\left(c_s^2\rho - P_{EOS}\right)}. \tag{5}$$

Due to the form of this self-interaction force, this pseudo-potential ψ allows the ideal LB EOS to be replaced with an arbitrary EOS $P_{EOS}(\rho)$ (Kupershtokh et al., 2009; Yuan and Schaefer, 2006).

Following earlier work (Kamali and Van Den Akker, 2013; Mukherjee et al., 2019b,a), we use the Carnahan-Starling EOS (CS-EOS) for the two main fluid components, denoted α and β. Compared with other EOSs, such as Van der Waals and Peng-Robinson, the CS-EOS has been found to have lower spurious currents along interfaces and better numerical stability (Zarghami et al., 2015). The CS-EOS is

$$P_{EOS} = \rho RT \frac{1 + b\rho/4 + (b\rho/4)^2 - (b\rho/4)^3}{(1 - b\rho/4)^3} - a\rho^2, \tag{6}$$

where a and b are attraction and repulsion parameters, respectively, and R is the component's gas constant, which is related to the universal gas constant R_u through $R = R_u/M$ in which M denotes the molecular mass of either main component. In this work, we use $a = 1$, $b = 4$, $R = 1$ which simplifies computations and has been found to provide satisfactory stability and interface thickness in LB simulations (Huang et al., 2011). With these parameter values, the critical temperature is $T_c = 0.09433$, the critical density is $\rho_c = 0.1304$, and the critical pressure is $P_c = 0.004417$. The reduced temperature, pressure, and density are defined as $T_r = T/T_c$, $P_r = P/P_c$, and $\rho_r = \rho/\rho_c$, respectively.

Since we consider systems in which the density of the surfactant s, being the third component, is small ($\rho_s \lesssim 0.02$), we use an ideal EOS for this component. The partial pressure of the surfactant is therefore

$$P^s = \rho^s R_s T, \tag{7}$$

where $R_s = R_u/M_s$ is the surfactant's gas constant, R_u is the universal gas constant, and M_s is the molecular mass of the surfactant. Variation in the choice of R_s, which we consider later, should therefore be interpreted as a change in the molecular weight of the surfactant. Though the EOS for the third component is ideal, it differs from the LB EOS, and this change in EOS is implemented through the self-interaction force, Eq. (4). In fact, in our LB implementation, we use the so-called β scheme which is a modified form of Eq. (4) given by

$$\vec{F}^\sigma = \beta\psi^\sigma(\vec{x}) \sum_i w_i \psi^\sigma(\vec{x} + \vec{e}_i)\vec{e}_i + ((1-\beta)/2) \sum_i w_i (\psi^\sigma(\vec{x} + \vec{e}_i))^2 \vec{e}_i \tag{8}$$

Use of this scheme (Kupershtokh et al., 2009; Zarghami et al., 2015) to evaluate the pseudo-potential interaction force has been shown to improve numerical stability and reduce spurious currents. It also provides a better agreement between the computed vapour-liquid densities and values for the CS-EOS as obtained via the Maxwell construction, in particular along its vapour branch, with an optimal value of $\beta = 1.25$ (Zarghami et al., 2015). Fig. 1 and particularly the inset show that running single-component simulations resulted in a similar finding about the effect of β. In our study on liquid–liquid dispersions in the absence of a vapour phase (see Section 3.2 below), we anyway used $\beta = 1.25$ throughout for all three components, all at $T_r = 0.95$.

In addition to their self-interaction, which specifies the EOS of the individual components, all components experience a force due to the other components that are present. The populations of the three components, α, β and surfactant s, are calculated on separate lattices, while they interact through body forces that describe intermolecular forces (Krüger et al., 2017; Huang et al., 2015; Chen et al., 2014). The force $\vec{F}^{\alpha,\beta}$ on component α due to component β is given by

$$\vec{F}^{\alpha,\beta} = -G_{\alpha\beta}\psi^\alpha(\vec{x}) \sum_i w_i \psi^\beta(\vec{x} + \vec{e}_i\Delta t)\vec{e}_i. \tag{9}$$

The strength of the interaction between components α and β is specified by the parameter $G_{\alpha\beta}$, denoted as the interaction strength, with a positive (negative) value indicating repulsion (attraction). For the calculation of the inter-component interactions, we use $\psi^\sigma = \rho^\sigma$ (different from Eq. (5)). The total intercomponent interaction force on component α is the sum of the contributions from all other components β. Due to the intra- and inter-component interactions, the total pressure in the multiphase, multicomponent system is (Krüger et al., 2017)

$$P = c_s^2 \sum_\sigma \rho^\sigma + \frac{c_s^2}{2} \sum_\sigma \sum_{\bar{\sigma}} G_{\sigma\bar{\sigma}} \psi^\sigma \psi^{\bar{\sigma}}. \tag{10}$$

The second sum includes all pairs of components, which includes the self-interaction terms for which $G_{\sigma\sigma} = -1$. Note that the definition of ψ is different for intra- and inter-component interactions.

In all simulations reported in this paper, all intra- and inter-component forces are incorporated by using the method of Guo et al. (2002). In our multicomponent multiphase system, use of the EDM (Kupershtokh et al., 2009) or Shan–Chen (Shan and Chen, 1993) forcing schemes with $G_{\alpha\beta} = 0$ led to phase separation within the vapour phase, an unphysical effect. This separation does not occur with the Guo scheme. In the Guo forcing scheme, the barycentric velocity $\vec{u}_b$, given by

$$\vec{u}_b = \frac{1}{\rho} \sum_\sigma \left(\rho^\sigma \vec{u}^\sigma + \frac{\vec{F}^\sigma}{2}\right), \quad \rho = \sum_\sigma \rho^\sigma, \tag{11}$$

is used as the equilibrium velocity of every component, i.e. $\vec{u}^\sigma = \vec{u}_b$ in Eq. (2) for all σ. Here, $\vec{F}^\sigma$ is the total force acting on component σ

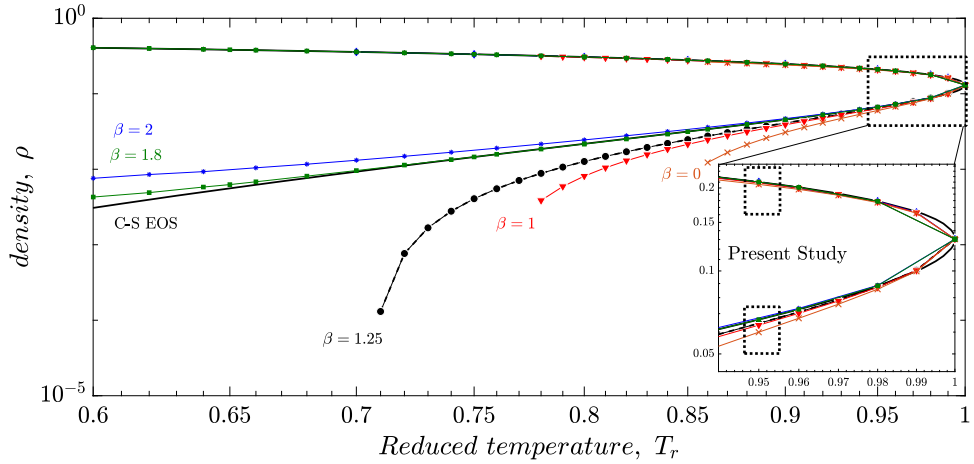

Fig. 1. Vapour and liquid densities for the C-S EOS as determined using the Maxwell construction (solid line) and the PPLB model with the β forcing scheme and varying values of the parameter β. In these single-component simulations, $\tau = 1$ and the force is implemented using the method of Guo. The dotted small black boxes in the insert show the specific reduced temperature for this study ($T_r = 0.95$).

according to the β-scheme of Eq. (8). The Guo scheme uses a power series expansion to discretize the force, resulting in the source term

$$S_i^\sigma = \left(1 - \frac{1}{2\tau^\sigma}\right) w_i \left(\frac{\vec{c}_i - \vec{u}}{c_s^2} + \frac{(\vec{c}_i \cdot \vec{u})\vec{c}_i}{c_s^4}\right) \cdot \vec{F}^\sigma \tag{12}$$

to be added to the right-hand side of the LB equation (Eq. (1)).

The modelling approach presented here offers several advantages over previous work (Mukherjee et al., 2019b,a). First, use of the Guo forcing scheme overcomes the instability of the Shan–Chen approach for low reduced temperatures ($T_r < 0.9$) and the unphysical separation of the gas phase for $G_{\alpha\beta} \to 0$. Additionally, instead of using three non-ideal fluids, an ideal EOS is used for the surfactant, which eliminates the computational expense of evaluating the CS-EOS for the third component. Though we do not pursue these topics in this paper, use of a non-ideal vapour-liquid EOS in the model offers two benefits: the possibility of simulating liquid–liquid systems with unequal densities (by specifying different molecular weights or critical temperatures for the components) and three-phase systems.

Finally, the implementation of PPLB for a three-component system in this study avoids the use of a factor S (as defined by Skartlien et al., 2011 and Mukherjee et al., 2019a) to scale the liquid-to-surfactant force. The motivation for this factor was to avoid instabilities at low surfactant densities; without this factor, Mukherjee et al. observed that a high surfactant density is needed to avoid such instabilities, as a result of which droplets of the surfactant component may form. Use of this scaling factor affects the conservation of momentum as pairwise momentum between the liquids and surfactant is not conserved for $S \neq 1$.

3. Simulating multicomponent systems in PPLB

In the sections that follow, we present the effects of various system parameters on the composition of the phases and interfacial tension between them before considering simulations of droplet deformation and breakup in the presence and absence of surfactants. First in Section 3.1, we describe the computational approach of this study, and then in Section 3.2, we describe the compositions of the two main liquids in a two-component PPLB simulation as a result of phase separation for varying values of PPLB's intermolecular interaction parameter. We then show in Section 3.3 how interfacial tension responds to the introduction of a surfactant as the third phase in then a three-component PPLB model for varying values of the interaction force $G_{\alpha\beta}$, among other parameters.

Section 4 then turns to the main topic of this paper: the role of a surfactant in shear driven droplet deformation and breakup and the underpinning (flow) behaviour of the surfactant in a thin interface layer during the ongoing deformation process. Finally, Section 5 presents the conclusions of this exploratory study on how to deal with a surfactant in a PPLB model and about the effect of a surfactant on droplet deformation and breakup.

3.1. Computational approach

We use the parallel, open-source LB code Palabos (Latt, 2009), which we adapted to implement a three-component system. Post processing and analysis of results is performed in Matlab. For all simulations, we use $\tau^\alpha = \tau^\beta = \tau^s = 1$, and therefore (see the text below Eq. (3)) the viscosity of the combined (multi-component) fluid is $\nu = \nu^\sigma = 1/6$.

We use simulations of spinodal decomposition to determine the phases present and their compositions as a result of the automatic phase separation caused by the intermolecular interactions modelled in PPLBM. Spinodal decomposition describes the rapid demixing of a mixture to form distinct phases. Two dimensional simulations of spinodal decomposition with two and three components in a periodic domain were performed. In these simulations, the initial density distribution of each component was random with 1% fluctuations around a specified average density ($\bar{\rho}^\alpha$, $\bar{\rho}^\beta$, and $\bar{\rho}^s$). The domain size was $n_x \times n_y = 75 \times 37$. Only those random initial conditions that led to the presence two flat interfaces that separate one region with primarily the α component and another with the β component were analysed.

Spinodal decomposition simulations were also used to determine the interfacial tension as a function of the components present, their properties, and the strengths of the interactions between them. For these simulations (without imposed flow), the domains were larger (75×75), and they proceeded until an equilibrium was achieved with a steady density distribution and one droplet present. The required equilibration time was $\approx 10^6$ time steps (approximately $30n_x^2/\nu$, where ν is an estimate of the rate of diffusion in this LB model). Note that surface tension is neither an input parameter nor a variable in the simulation. A posteriori, the Young–Laplace equation can be used to find a value for the interfacial tension γ, i.e. $\gamma = R\Delta P$, where $\Delta P = P_i - P_o$ is the difference in pressure between the interior (P_i) and exterior (P_o) of the droplet, and R is the droplet radius. To determine the radius of the droplet, the position of its interface is considered to be located where $\rho^\alpha = \rho^\beta$.

3.2. Phase behaviour of the two main components

Since the third (surfactant) component will only be present in small amounts, we evaluate first the composition of the coexisting phases in

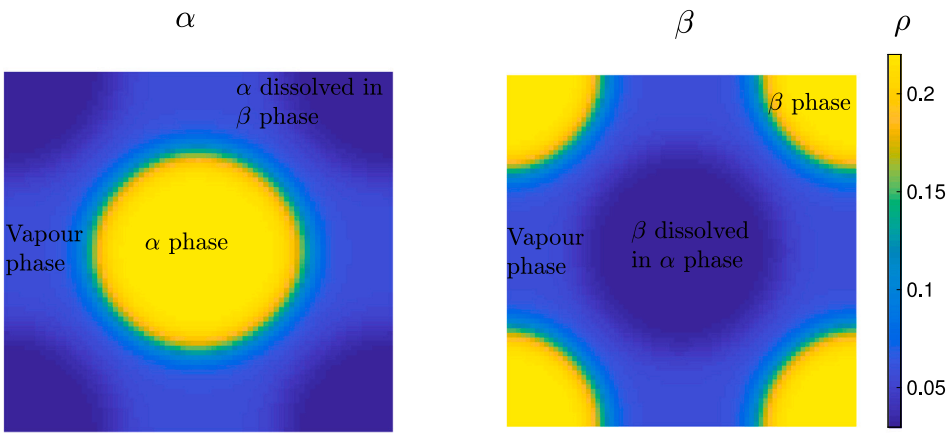

Fig. 2. Sample density distributions for a two-component system showing two liquid phases surrounded by a vapour phase. The average densities of the α and β components are equal ($\bar{\rho}^{\alpha} = \bar{\rho}^{\beta} = 0.09$), $T_r^{\alpha} = T_r^{\beta} = 0.95$, and $G_{\alpha\beta} = 0.5$.

a two-component system. In these studies, we use simulations with a negligible average surfactant density ($\bar{\rho}_s = 10^{-6}$) as surrogates for truly two-component (surfactant-free) systems for simplicity in the numerical implementation. To our knowledge, the behaviour of a system with two non-ideal components that follow the CS-EOS together with inter-component interactions with a surfactant based on $\psi = \rho$ has not been previously reported.

Depending on the amounts of the two components present, their reduced temperatures, and the strength of the interactions between them, up to three phases could be present at equilibrium for a two-component system: two liquid phases and a vapour phase. Sample density distributions for such a case with three phases are shown in Fig. 2. We see that in the droplet of the α phase, a small amount of β is dissolved, which appears as a dark blue region in the distribution of the β component. Similarly, a small amount of α is in the droplet with mostly β, which is centred at the corners of the periodic domain. The surfaces of the droplets are diffuse which is a characteristic of PPLB simulations (Engblom et al., 2013; Mukherjee et al., 2019a). For this simulation, the average densities are $\bar{\rho}^{\alpha} = \bar{\rho}^{\beta} = 0.09$, which is less than the critical density. The densities of both components in the vapour phase are equal. The vapour phase densities lie in between the densities found in the liquid droplets.

Since we focus on liquid–liquid systems in this paper, the average densities of the components were chosen to be sufficiently high that a vapour phase cannot form. For example, if the CS-EOS gives the liquid phase density ρ^L at a particular T_r, the average densities of the two components that will yield a volume fraction ϕ for the phase that is rich in the α component can be estimated using:

$$\bar{\rho}^{\alpha} \approx \phi\rho^L \tag{13}$$

$$\bar{\rho}^{\beta} \approx (1-\phi)\rho^L \tag{14}$$

This estimate assumes that the vapour phase density at these conditions is small compared to the density of the dominant component in each liquid phase, and also the dissolved amount of the non-dominant component in each phase is negligible. Once the compositions of the coexisting liquid phases are known for a particular $G_{\alpha\beta}$ and T_r, the required average densities to achieve a volume fraction ϕ can be estimated more accurately using

$$\bar{\rho}^{\alpha} \approx \phi\rho_{\alpha}^L + (1-\phi)\rho_{\alpha}^D \tag{15}$$

$$\bar{\rho}^{\beta} \approx (1-\phi)\rho_{\beta}^L + \phi\rho_{\beta}^D \tag{16}$$

where ρ_i^L is the density of component i in the phase in which it is dominant, and ρ_i^D is the dissolved amount of component i in the other phase.

In this paper, we consider only symmetric systems in which the two components have the same properties (same EOS and parameters); these equations are readily generalized for components with different properties. As a result, the densities of the dominant and dissolved components in each phase are equal and only their identities are exchanged, i.e. $\rho_{\alpha}^L = \rho_{\beta}^L$ and $\rho_{\alpha}^D = \rho_{\beta}^D$.

Fig. 3 presents the observed densities in a series of simulations with varying T_r (same for both components) and $G_{\alpha\beta}$. For these spinodal decomposition simulations, each component was initialized with random 1% variation around average densities of $\bar{\rho}^{\alpha} = 0.16$ and $\bar{\rho}^{\beta} = 0.13$. Since the system is symmetric (both components are identical), this figure shows the composition of either phase that forms.

For weak interaction strengths ($G_{\alpha\beta} = 0.01$), each component behaves independently of the other component, rach separating into a liquid and a vapour phase. In this limit of low $G_{\alpha\beta}$, we compare the observed densities with analytical results for the CS-EOS. For $T_r \geq 0.9$, the phase compositions are in good agreement with the analytical liquid and vapour densities for the CS-EOS. In the inset of Fig. 3, we see that the reduced pressures in the binary mixture for $G_{\alpha\beta} = 0.01$ the (blue curve) are approximately double those of the CS-EOS for one component (the black curve).

With higher values of $G_{\alpha\beta}$, only two liquid phases form. This contrasts with the conditions of Fig. 2, where the lower average densities allowed a vapour phase to form. The black squares in Fig. 3 show the densities of the phases in the liquid–liquid–vapour system that was shown in Fig. 2. We see that the densities in the liquid phases are similar in both cases, and the vapour density in the liquid–liquid–vapour system is similar to the expected value from the CS-EOS.

Phase separation occurs up to $T_r = 1.07$ and 1.15 for $G_{\alpha\beta} = 0.5$ and 1, respectively. As is evident from the right side of Fig. 3 and its inset, the critical solution temperature for the two-component system increases with increasing $G_{\alpha\beta}$. Above this critical temperature, two liquid phases no longer form, and the two components are miscible. The inset of Fig. 3 shows how the $P-T$ curves shift up and to the right with increasing $G_{\alpha\beta}$. The endpoint of each curve is at the critical solution temperature, and we see that this point shifts to higher temperatures and pressures with increasing $G_{\alpha\beta}$. In the region with $T_r > 1$, we see phase separation *above* the critical temperature of either pure component, which is similar to a phenomenon called "gas–gas immiscibility" and observed experimentally (van Konynenburg and Scott, 1980).

3.3. Effect of surfactant on interfacial tension

We then ran PPLB simulations with three components, the third component being the surfactant at a concentration lower than the CMC such that the formation of micelles is not taking place. By a proper choice of the mutual G-values, the surfactant collects at the interface between the two liquid phases, with all components varying

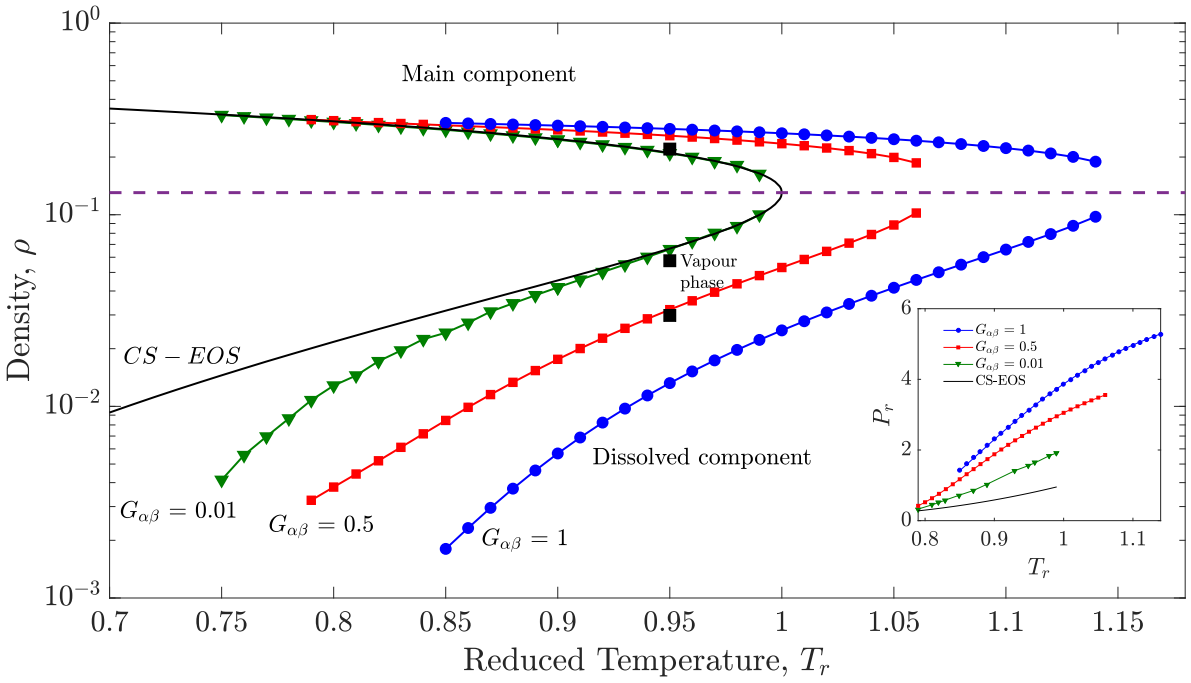

Fig. 3. Composition of the liquid phases in the simulated symmetric two-component system as a function of the interaction strength $G_{\alpha\beta}$ and the reduced temperature T_r. For both liquid phases, the upper branch shows the density of the dominant component, while the lower branch shows the dissolved amount of the other component, all depending on the value of $G_{\alpha\beta}$. The three black squares show the densities of the phases in the sample liquid–liquid–vapour system shown in Fig. 2. The horizontal (dashed purple) line shows the critical density. The inset shows the relationship between reduced pressure and temperature for the same data points as in the main figure. (For interpretation of the references to colour in this figure legend, the reader is referred to the web version of this article.)

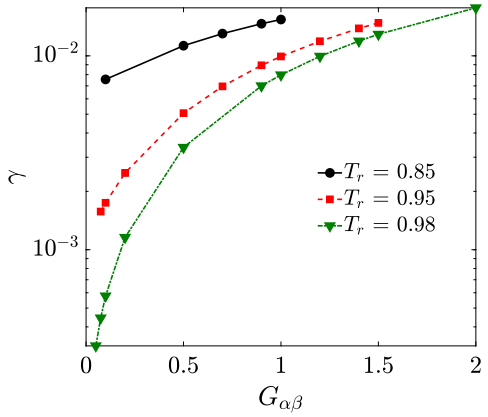

Fig. 4. Interfacial tension between liquid phases as a function of $G_{\alpha\beta}$ and T_r in a two component system with $\bar{\rho}^{\alpha} = 0.13$ and $\bar{\rho}^{\beta} = 0.16$.

diffusely across the droplet interface, just as reported by Mukherjee et al. (2019a).

To provide reference data with which we can compare the three-component results, we first examine the effects of the model parameters on the interfacial tension in a clean, i.e. surfactant-free, system. Fig. 4 shows the interfacial tension as a function of $G_{\alpha\beta}$ for several reduced temperatures. Consistent with the behaviour of a single component, interfacial tension increases with decreasing T_r. As the repulsive force between the components is increased, the interfacial tension between the liquid phases increases.

We consider now how adding small amounts of a third component changes the interfacial tension. We vary $\bar{\rho}^{\alpha}$ and $\bar{\rho}^{s}$ over the ranges $\bar{\rho}^{\alpha} \in [0.063, 0.14]$ and $\bar{\rho}^{s} \in [10^{-6}, 0.02]$ while keeping $\bar{\rho}^{\beta} = 0.147$. The system temperature is $T = 0.0896$, and therefore $T_r^{\alpha} = T_r^{\beta} = 0.95$. We use $R_s = 1.57$, $G_{\alpha\beta} = 1$, $G_{\beta s} = G_{\alpha s} = 0.8$. We have also investigated, but do not report at this stage, the effects of changes in R_s, $G_{\alpha\beta}$, $G_{\beta s}$, and $G_{\alpha s}$. The choice of maximum $\bar{\rho}^{s}$ is limited by the formation of a surfactant phase or stability of the numerical method. In all simulations, the viscosity of all components (and therefore phases) is the same ($\tau^{\alpha} = \tau^{\beta} = \tau^{s} = 1$). To have equal amounts of surfactant in the dispersed and continuous phases, we use $G_{\beta s} = G_{\alpha s}$.

Fig. 5(a) shows that the interfacial tension (in LB units) remains effectively constant upon adding (small) amounts of surfactant, increasing by just 1% with increasing $\bar{\rho}^{s}$ with all other parameters kept constant. Due to increasing mass in a fixed volume, the pressure (see Fig. 5(b)) also increases with increasing amount of the surfactant (Eq. (10)). Considering the limit of negligible $\bar{\rho}^{s}$ in Fig. 5(a) and (b), we see that interfacial tension in the two-component PPLB model increases with increasing density of the components present (in this case increasing $\bar{\rho}^{\alpha}$) and therefore the system pressure.

The effect of adding the third component is also to (marginally) increase the pressure, which then is also expected to raise the interfacial tension (as when increasing ρ^{α}). Fig. 5(a), however, shows that the interfacial tension remains constant with increasing $\bar{\rho}^{s}$. Therefore any increases in interfacial tension due to increasing pressure (due to increasing $\bar{\rho}^{s}$) are offset by a decrease due to the presence of the third component.

The reduction of interfacial tension due to a surfactant in PPLB strongly depends on the G-values used for mimicking the mutual interaction between the components and on the value of the molecular mass of the surfactant (leading to variations in R_s). As this was already found in our earlier PPLB simulations (Mukherjee et al., 2019a), this effect is outside the scope of this study. In this paper, we focus on the occurrence of an uneven spatial surfactant distribution and its effect on droplet deformation and breakup in a shear flow. Such an phenomenon was observed earlier in our studies on droplet formation at an aperture where the surfactant during the fall of a droplet was driven to the droplet's tail (Mukherjee et al., 2019a).

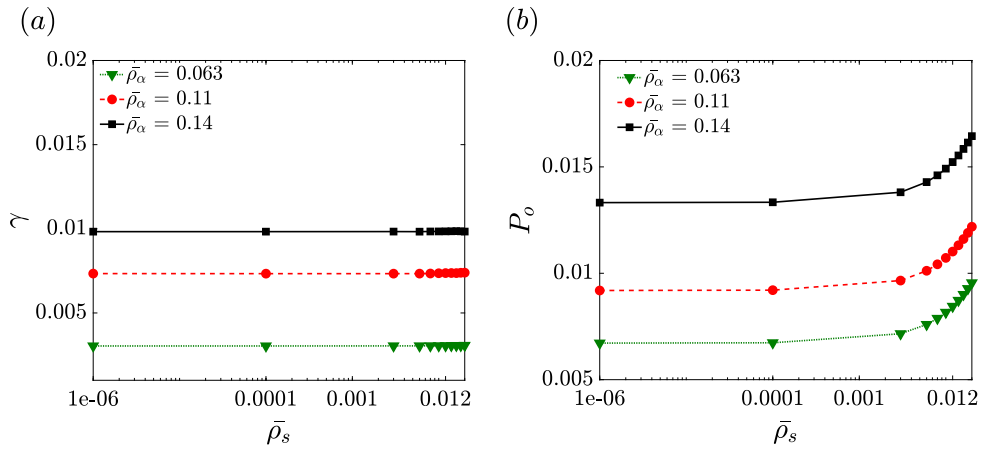

Fig. 5. (a) Interfacial tension and (b) external (continuous phase) pressure as a function of the amount of surfactant ($\bar{\rho}^s$) for several $\bar{\rho}^\alpha$, for $T_r^\alpha = T_r^\beta = 0.95$, $R_s = 1.57$, $G_{\alpha\beta} = 1$, $G_{\beta s} = G_{\alpha s} = 0.8$, $\bar{\rho}^\beta = 0.147$.

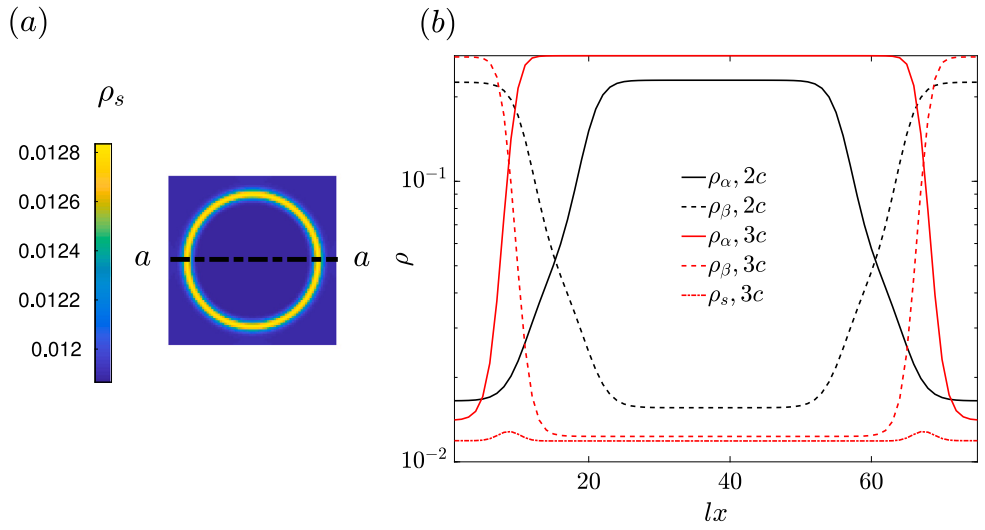

Fig. 6. (a) Surfactant density distribution along the interface of a droplet; (b) Density profiles of α, β and surfactant across the diameter of a droplet for two (2c) and three (3c) component systems. Solid lines show the dispersed phase density, dashed lines show the continuous phase density, and the dash dotted line shows the surfactant density. The simulation parameters are $T_r^\alpha = T_r^\beta = 0.95$, $R_s = 1.57$, $G_{\alpha\beta} = 1$, $G_{\beta s} = G_{\alpha s} = 0.8$, $\bar{\rho}^\beta = 0.147$.

3.4. Interface thickness

In this model, the interface thickness is O(10), defined as the distance over which 95% of the change in density occurs. Fig. 6 shows for a typical case ($T_r^\alpha = T_r^\beta = 0.95$, $R_s = 1.57$, $G_{\alpha\beta} = 1$, $G_{\beta s} = G_{\alpha s} = 0.8$, $\bar{\rho}^\beta = 0.147$) that adding surfactant steepens the density profiles of the two main components at the interface. The steeper interface profiles of the main components would indicate that interfacial tension is higher, but this increase is offset by the presence of the surfactant, and the net result is the minimal change in interfacial tension discussed in the preceding section.

4. Droplet deformation and breakup in shear

4.1. Introduction and validation

The presence of surfactant has two main effects on an interface. The first consequence is a lowering of the (average) interfacial tension. The second is the introduction of Marangoni stresses due to variation in surfactant concentration along the interface. These tangential stresses act in the direction from regions of high surfactant concentration (low tension) to lower surfactant concentration (higher tension). As a result, the shape of a droplet in shear flow, the distribution of surfactant, and the flow patterns in and outside the droplet are tightly coupled. In this section, we assess the effects of variation in surfactant concentration on droplet deformation and breakup in shear. To isolate the effect of variation in surfactant concentration from the effect of a lower interfacial tension, we choose parameters so that we compare cases with the same interfacial tension. For the cases with surfactant, this is the (uniform) interfacial tension at rest before the shear flow is started.

Whether a droplet breaks apart in a shear flow or, if it does not break, which form it takes, depends on the ratio of viscous and interfacial stresses called the capillary number. The capillary number is defined as $\mathrm{Ca} = \frac{\mu\dot{\gamma}R}{\gamma}$, and R is the droplet radius. With increasing Ca, droplets deform to a greater extent, and when a critical value $\mathrm{Ca_c}$ is exceeded, they break. The shape and critical capillary number for breakup also depend on the droplet Reynolds number ($\mathrm{Re} = \dot{\gamma}R^2/\nu$). In this section, we assess how the shape of a droplet changes due to the presence of surfactant while keeping the capillary number constant. We also evaluate how the surfactant affects $\mathrm{Ca_c}$ and the breakup process.

To validate our PPLB simulation method, we first compute steady droplet shapes for the two-component system at the three capillary numbers 0.2, 0.4, and 0.6, with the droplet Reynolds number being fixed at one. The droplet diameter is 32 lattice units in a 256×129 domain, and all steady droplet shapes are captured after $5{\times}10^6$ simulation

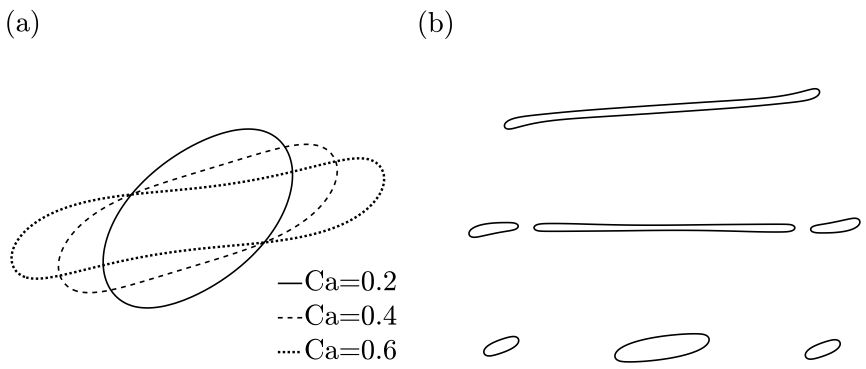

Fig. 7. (a) Steady droplet shapes for several Ca (0.2, 0.4 and 0.6) and Re = 1; (b) Droplet break-up for Ca = 1.4 and Re = 1.

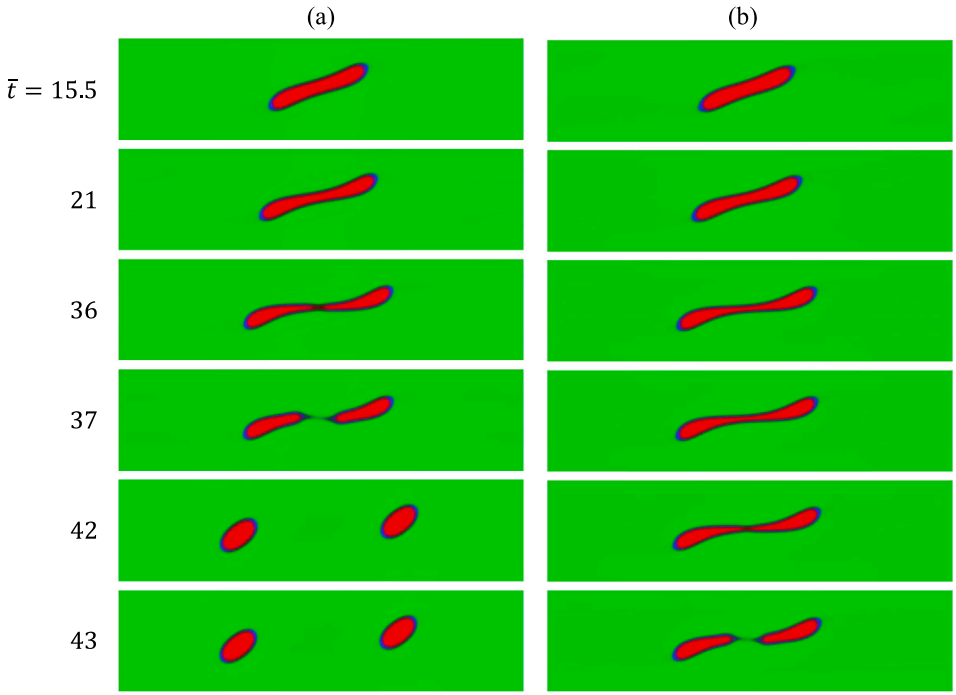

Fig. 8. Effect of surfactant on droplet break-up at various moments in time $\bar{t} = \dot{\gamma}t$. (a) Sample simulation without surfactant and supercritical Ca = 0.271 and Re = 6.5 (b) Same Ca as (a) but with surfactant and Re = 6.45 ($\bar{\rho}^s = 0.012$, $\bar{\rho}^\alpha = 0.07415$). The compositions of the phases for these simulations can be found in Table 1. Initial droplet size was 40 l.u.

time steps. The BGK relaxation times for all fluids are the same, and the values are 1.7, 2.204 and 2.58 for $Ca = 0.2$, 0.4 and 0.6, respectively. All simulations are for two liquids with equal densities and viscosities.

Fig. 7(a) demonstrates that as Ca increases, droplet deformation increases, in good agreement with simulations by Zong et al. (2020) by means of a phase field approach, while Fig. 7(b) shows that at $Ca = 1.4$ and $Re = 1$, the droplet breaks up into several droplets. This is in good agreement with snapshots reported by Van der Sman and Van der Graaf (Van der Sman and Van der Graaf, 2008) on the basis of free energy LB simulations. The critical capillary number for breakup is found to be $Ca_c \approx 0.21$ near $Re = 7$. This compares favourably with Li et al. (2000) who found in VOF simulations that droplets break up at $Ca = 0.2$ for $Re = 4$ and at $Ca = 0.15$ for $Re = 10$. Komrakova et al. (2014) using a free-energy LB method reported $Ca_c = 0.165$ at $Re = 10$ and $Ca_c = 0.285$ at $Re = 1$, while Khismatullin et al. (2003) obtained similar values by using a VOF technique. Given the spread in the results from the various computational studies, our conclusion is that our PPLB method produces critical capillary numbers in the right range.

4.2. The effect of surfactant on breakup times

For the simulations of droplet deformation and break-up in shear, the domain size was 801 × 201 due to the elongation of the droplet before break-up. To study the effects of varying the amount of surfactant on droplet deformation and break-up, we compare simulations with and without surfactant but at the same capillary number and the same Reynolds number, viz. at Ca = 0.271 and Re = 6.5. Fig. 8(a) shows the result for the surfactant-free system. In this case, the droplet splits into two droplets at $\bar{t} = \dot{\gamma}t = 37$. At the same capillary number but with $\bar{\rho}^s = 0.012$ (Fig. 8(b)), we see that breakup is delayed until $\bar{t} = 43$. Hence, at Ca = 0.271 and Re = 6.5, we find that addition of surfactant delays breakup. This is, however, not always the case.

To further investigate this phenomenon, we ran simulations over a range of supercritical Ca values. The dependence of non-dimensional breakup time $\dot{\gamma}t$ on Ca and the presence of surfactant is shown in Fig. 9. In general, we see two curves shifted with respect to each other. This means that due to the addition of surfactant the overall behaviour for a clean interface is shifted to higher Ca values. For values of Ca that

Table 1
Composition of the dispersed (superscript d) and continuous (c) phases for the cases shown in Fig. 8. The last two columns provide the total densities of the dispersed and continuous phases. All values are determined after equilibration (3×10^6 time steps) and before shear starts.

Case	ρ^d_α	ρ^c_α	ρ^d_β	ρ^c_β	ρ^d_s	ρ^c_s	ρ^d_{total}	ρ^c_{total}
Fig. 8 (a)	0.2329	0.01588	0.01516	0.2305	–	–	0.2481	0.2564
Fig. 8 (b)	0.2344	0.01583	0.01512	0.232	0.01192	0.01196	0.2615	0.2598

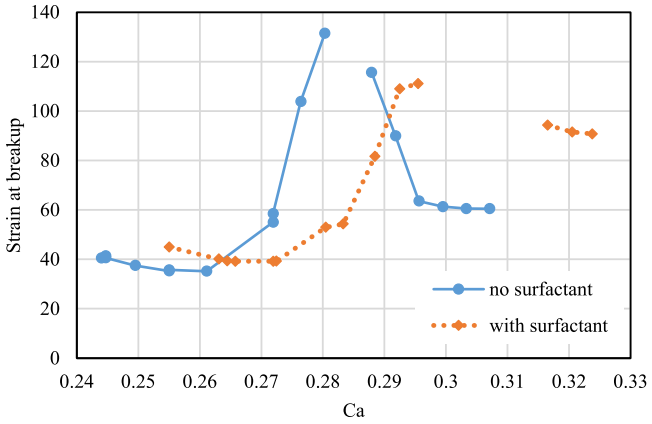

Fig. 9. Changes in droplet breakup time with increasing capillary number for droplets with ($\tilde{\rho}^s = 0.01236$) and without surfactant. Initial drop size was 40 l.u.

are slightly supercritical (say, in excess of 0.2), the time until breakup increases with increasing Ca. For these values of Ca, the initial droplet splits into two droplets. If the capillary number is increased further, the initial droplet breaks into three droplets, and the time to breakup decreases. The critical capillary numbers for breakup into both two and three droplets are higher in simulations with surfactant than without.

In this Fig. 9, the capillary numbers are calculated using the interfacial tension of the initial single droplet at rest after equilibration, i.e. before shear is started. If the effect of adding a surfactant on droplet breakup were a reduction of the average interfacial tension only, a single curve would result in Fig. 9. The figure therefore shows the additional effects of the surfactant beyond a reduction in average interfacial tension. The observed shift to higher Ca indicates that stronger shear stresses are needed to break a surfactant-coated droplet than one that has a clean interface and the same average interfacial tension. Similar effects were reported by Liu et al. (2018) for insoluble surfactants.

The evident need for higher shear to obtain the same droplet breakup time is indicative of extra forces resisting the breakup or mitigating the impact of the shear. This reminds us of the role of Marangoni stresses as a result of inhomogeneous surfactant concentrations along an interface. Note that in PPLB, Marangoni stress is not an explicit input parameter of the simulations, similar to how interfacial tension is not specified directly. A characteristic feature of PPLB simulations is that the behaviour is defined in terms of intra- and inter-component forces (see Eqs. (4), (8), (9), (11) and (12)). Eq. (9) establishes that the local forces on the primary components depend on the local surfactant concentration, which is the origin of spatially varying interfacial forces and therefore Marangoni stresses in our model. The indirect a posteriori evidence that Marangoni stresses are part of the PPLB solution is in Fig. 9: if we did not have Marangoni stresses, the 'with surfactant' findings would be the same as the 'no surfactant' results (unless there is unexpected behaviour in the model). In addition, breakup is delayed (see Fig. 8). Because the results are consistent with studies that explicitly include Marangoni effects, we consider our results sound and not a model defect. In our view, the (automatic) inclusion of the Marangoni stresses is related to the inherent and spontaneous phase redistribution and separation in PPLB.

4.3. Surfactant distribution due to shear

We ran a transient PPLB simulation of the breakup of a droplet loaded with a surfactant. In this case, the capillary number $Ca = 0.255$ was low enough to get simple binary breakup, as reported by Zhang et al. (2021). According to De Bruijn (1993), our surfactant concentration was sufficiently high to prevent tip streaming from occurring. The snapshots in Fig. 10 from this transient simulation show how the surfactant distribution evolves along the interface of a droplet during deformation and breakup. Under the action of the shear stresses exerted upon the droplet by the flow field, the droplet is deformed and stretched while the surfactant is transported from the middle of the droplet (where later breakup will occur) towards the tips of the deforming droplet where it reduces the local interfacial tension. In the middle of the stretched droplet, a neck is formed that breaks up after a pause during which the surfactant continues to redistribute. After breakup, the two droplets regain a similar elliptical shape with again a non-uniform surfactant distribution and interfacial tension. Given the shift between the two curves in Fig. 9, these inhomogeneous surfactant concentrations evidently result in (Marangoni) stresses mitigating the effect of shear.

Our observations from these PPLB simulations are in line with the observations reported by Liu et al. (2018) on the basis of their hybrid LB and finite–difference simulations of droplet dynamics with insoluble surfactants. The breakup process in our current simulations resembles the necking and pinch-off process of a droplet formed at an orifice as reported earlier (Pozrikidis, 2012; Berghout and Van den Akker, 2019; Van den Akker et al., 2021). Overall, there is a good agreement with the observations reported by Liu et al. (2018) on deformation, breakup and surfactant concentrating at the tips for capillary numbers in the same range as ours.

Fig. 10, just like Fig. 7(b) and Fig. 8, illustrates the benefits of diffuse interface simulations such as PPLB. Diffusion regularizes the singularities of sharp interface models and allows such simulations where topological changes are a consequence of the model equations. Simulations of droplet breakup and coalescence with LB and FV techniques are widely reported in the literature. Here we focus on surfactant modelling within a framework that can conveniently handle topological changes. Also with this three component PPLB, we even track the evolution of surfactant concentrations during topological changes — see also e.g. Mukherjee et al. (2019a).

Fig. 11 once more shows the spatial distribution of the surfactant along with the flow field outside and inside the droplet in high–resolution detail for a droplet with Taylor deformation parameter $D = (L - B)/(L + B) = 0.45$. The shape of the droplet and its internal recirculatory flow resembles a case ($Ca = 0.265$, $D = 0.43$, low drop viscosity) reported by Bazhlekov et al. (2006). The D values reported by Zhou et al. (2023) are some 10% lower.

This figure is in general agreement with the (mainly) experimental observations on the transport of a surfactant at the interface of a shear driven deforming droplet as reported by e.g., Janssen et al. (1994b,a) and Feigl et al. (2007). These authors reported about the deformation, the internal circulation inside the droplet, and the flow of surfactant inside a thin interface layer with varying surfactant concentration due to diffusive transport into the bulk of the droplet. All these aspects are confirmed in Fig. 10. A key advantage of our PPLB approach is its ability to track the evolution of surfactant concentration during topological changes. As a result, our figures reveal much more detailed information

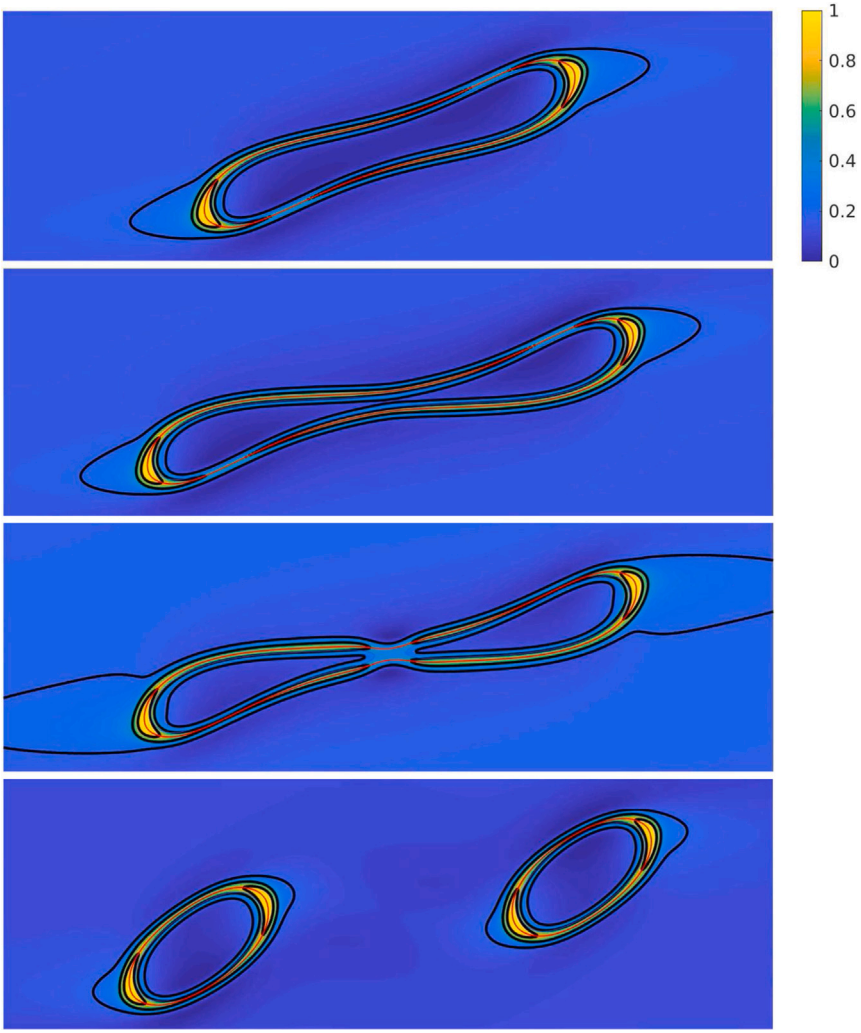

Fig. 10. Normalized surfactant concentration during breakup of a droplet at $Ca = 0.255$. Four times are shown (top to bottom): during initial deformation ($\bar{t} = 9.5$ after the start of the shear flow), during stretching of the neck ($\bar{t} = 41.8$), several time steps before breakup ($\bar{t} = 44.8$), and after separation ($\bar{t} = 50.7$). The interaction strengths are $G_{\alpha\beta} = 1$ and $G_{\alpha s} = G_{s\beta} = 0.8$. The surfactant concentration is $\bar{\rho}^s = 0.012$, and the initial droplet radius was 40. Only the region near the droplets is shown; the full domain size is 801 × 201, and the initial droplet radius is 40.

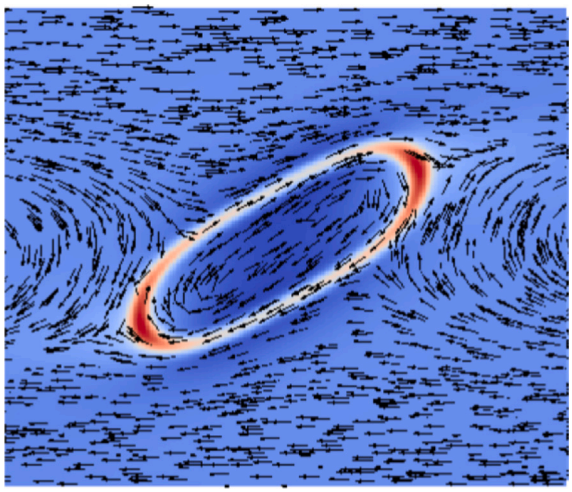

Fig. 11. Structure of the velocity field in and around a droplet with surfactant (blue to red shows low to high surfactant density). (For interpretation of the references to colour in this figure legend, the reader is referred to the web version of this article.)

about surfactant distribution during deformation and breakup than provided in earlier papers or is available from experiments.

Our computational method elegantly exploits a full PPLB method for both the flow field around the droplet and the surfactant transport and redistribution at the droplet's interfaces. In PPLB, the formation and evolution of phase interfaces are captured automatically, as molecular interactions are incorporated as the driving force for phase separation. In addition, unlike mesh-based methods, the PPLB approach allows for a straightforward treatment of topological changes, i.e. merging and splitting of interfaces. As a result, the PPLB approach is closer to physics and mathematically simpler. As such, our approach is also very different from those of Renardy et al. (2002), Yun et al. (2014), Liu et al. (2018) and Zhang et al. (2021) who all proposed and applied sophisticated computational models without producing the same detailed pictures of flow fields combined with surfactant distributions. Our results confirm the potential of our approach for dealing with a surfactant, as reported earlier by Mukherjee et al. (2019a).

An issue that still needs further investigation is how these exploratory computational results relate to real-world droplet break-up and real-world emulsions. In PPLB, interfacial tension is the resultant of the simulation, also in a three-component system where the surfactant, due to properly chosen values for the interaction strengths G, collects at the interface (see also e.g. Mukherjee et al., 2019a). A trial-and-error

method may have to be used to find the proper surfactant concentration and the proper G values.

A next step would be about finding out how to relate the values of our (successful) input parameters, particularly the various G values, to real-world physical properties and flow variables. The break-up case reported in this were obtained for $Re = 1$ and $Ca = 0.255$, with all G values of $O(1)$. Further study is required to determine how to run simulations for emulsions with relevant droplet sizes susceptible to deformation and break-up as a function of Re and the property group $Re/Ca = \gamma R/(\rho\nu^2)$ with properly chosen G values. This was beyond the scope of this exploratory study which focused on how to simulate in a PPLB model droplet break-up due to shear in the presence of a surfactant and on whether we could observe in PPLB the behaviour of the surfactant during the deformation and break-up process.

5. Conclusions

Our three-component PPLB model is capable of reproducing important aspects of the role and behaviour of a surfactant in the shear driven deformation and breakup of a liquid droplet immersed in an immiscible second liquid. Our method was implemented on the parallel, open-source LB code Palabos, with post-processing in Matlab. We first investigated and reported the phase separation and phase behaviour of the two main liquid components. Next, the liquid–liquid system was extended by adding a surfactant. The effect of stepwise adding increased amounts of the surfactant on the interfacial tension between the two main component was assessed. We found that the interfacial tension remains constant with increasing surfactant concentration due to competition between phenomena that increase and decrease interfacial tension.

The eventual focus of our research was on the role and behaviour of a surfactant during the shear driven deformation and breakup of an immiscible liquid drop. Our method shows the surfactant concentrating in a thin interface layer (as it should be), as in our method it is repelled by both main liquid components — in agreement with earlier findings (obtained with partly different methods) reported by Skartlien et al. (2011), Mukherjee et al. (2019a) and Van den Akker (2018).

Adding a surfactant not only reduces the average interfacial tension, it also induces further effects in the case of flow. The shear flow drives the surfactant to concentrate at the far ends of the deformed droplet and may reduce there the local interfacial tension while increasing the surfactant concentration halfway along the elongated droplet. The result of this inhomogeneous surfactant distribution along the interface is also that a higher shear is needed for droplet breakup and that breakup is delayed. Evidently, Marangoni stresses (opposing the shear driven flow) are captured inherently in our multicomponent PPLB simulations. In fact, this finding is part of the novelty of our paper.

During the increasing deformation, a continuous redistribution of the surfactant takes place up to the moment the droplet breaks up. The simulation results reveal the flow field of the external liquid phase, the internal circulation of the inner liquid, and the flow with surfactant gradients within the thin interface layer.

CRediT authorship contribution statement

Mohammad Pourtousi: Writing – original draft, Validation, Software, Investigation, Formal analysis. **Arman Safdari:** Writing – original draft, Validation, Software, Investigation, Formal analysis. **Orest Shardt:** Writing – review & editing, Validation, Supervision, Software, Investigation, Formal analysis, Conceptualization. **Harry E.A. Van den Akker:** Writing – review & editing, Validation, Supervision, Resources, Methodology, Funding acquisition, Formal analysis, Conceptualization.

Declaration of competing interest

The authors declare that they have no known competing financial interests or personal relationships that could have appeared to influence the work reported in this paper.

Acknowledgements

This research was conducted with the financial support of SSPC, the Taighde Éireann – Research Ireland Centre for Pharmaceuticals, funded by SFI and co-funded by the European Regional Development Fund, under Grant Number 14/SP/2750 .

Data availability

Data will be made available on request.

References

Adami, S., Hu, X.Y., Adams, N.A., 2010. A conservative SPH method for surfactant dynamics. J. Comput. Phys. 229 (5), 1909–1926.

Bazhlekov, I.B., Anderson, P.D., Meijer, H.E.H., 2006. Numerical investigation of the effect of insoluble surfactants on drop deformation and breakup in simple shear flow. J. Colloid Interface Sci. 298, 369–394.

Berghout, P., Van den Akker, H.E.A., 2019. Simulating drop formation at an aperture by means of a multi-component pseudo-potential lattice Boltzmann model. Int. J. Heat Fluid Flow 75, 153–164.

Chen, S., Doolen, G.D., 1998. Lattice Boltzmann method for fluid flows. Annu. Rev. Fluid Mech. 30, 329–364.

Chen, L., Kang, Q., Mu, Y., He, Y.L., Tao, W.Q., 2014. A critical review of the pseudopotential multiphase lattice Boltzmann model: Methods and applications. Int. J. Heat Mass Transfer 76, 210–236.

Chen, Z., Tsai, P., Komrakova, A., 2023. Dynamics of surfactant-laden drops in shear flow by lattice Boltzmann method. Phys. Fluids 35, 122119.

De Bruijn, R., 1993. Tipstreaming of drops in simple shear flows. Chem. Eng. Sci. 48, 277–284.

de Jesus, W.C., Roma, A.M., Pivello, M.R., Villar, M.M., Silveira-Neto, A., 2015. A 3D front-tracking approach for simulation of a two-phase fluid with insoluble surfactant. J. Comput. Phys. 281, 403–420, URL http://dx.doi.org/10.1016/j.jcp.2014.10.021.

Engblom, S., Do-Quang, M., Amberg, G., Tornberg, A.-K., 2013. On diffuse interface modeling and simulation of surfactants in two-phase fluid flow. Commun. Comput. Phys. 14 (4), 879–915.

Feigl, K., Megias-Alguacil, D., Fischer, P., Windhab, E., 2007. Simulation and experiments of droplet deformation and orientation in simple shear flow with surfactants. Chem. Eng. Sci. 62, 3242–3258.

Guo, Z., Zheng, C., Shi, B., 2002. Discrete lattice effects on the forcing term in the lattice Boltzmann method. Phys. Rev. E 65 (4), 046308.

Huang, H., Krafczyk, M., Lu, X., 2011. Forcing term in single-phase and Shan-Chen-type multiphase lattice Boltzmann models. Phys. Rev. E 84 (4), 046710.

Huang, H., Sukop, M., Lu, X., 2015. Multiphase lattice Boltzmann methods: Theory and application. John Wiley & Sons.

Huang, H., Thorne, Jr., D.T., Schaap, M.G., Sukop, M.C., 2007. Proposed approximation for contact angles in Shan-and-Chen-type multicomponent multiphase lattice Boltzmann models. Phys. Rev. E 76 (6), 066701.

Janssen, J., Boon, A., Agterof, W., 1994a. Droplet break-up in simple shear flow in the presence of emulsifiers. Colloids Surfaces A: Physicochem. Eng. Asp. 91, 141–148.

Janssen, J., Boon, A., Agterof, W., 1994b. Influence of dynamic interfacial properties on droplet breakup in simple shear flow. AIChE J. 40 (12), 1929–1939.

Kamali, M.R., Van Den Akker, H.E.A., 2013. Simulating gas-liquid flows by means of a pseudopotential lattice Boltzmann method. Ind. Eng. Chem. Res. 52 (33), 11365–11377.

Khismatullin, D.B., Renardy, Y., Cristini, V., 2003. Inertia-induced breakup of highly viscous drops subjected to simple shear. Phys. Fluids 15, 1351–1354.

Kian Far, E., Gorakifard, M., Mojtaba, G.F., 2023. A new three dimensional cumulant phase field lattice Boltzmann method to study soluble surfactant. Phys. Fluids 35, 053338.

Komrakova, A.E., Shardt, O., Eskin, D., Derksen, J.J., 2014. Lattice Boltzmann simulations of drop deformation and breakup in shear flow. Int. J. Multiph. Flow 59, 24–43.

Krüger, T., Kusumaatmaja, H., Kuzmin, A., Shardt, O., Silva, G., Viggen, E.M., 2017. The lattice Boltzmann method. In: Graduate Texts in Physics, Springer International Publishing.

Kupershtokh, A.L., Medvedev, D.A., Karpov, D.I., 2009. On equations of state in a lattice Boltzmann method. Comput. Math. Appl. 58 (5), 965–974.

Latt, J., 2009. Palabos, parallel lattice Boltzmann solver. FlowKit, Lausanne, Switzerland.

Lee, J., Pozrikidis, C., 2006. Effect of surfactants on the deformation of drops and bubbles in Navier–Stokes flow. Comput. Fluids 35 (1), 43–60.

Li, J., Renardy, Y., Renardy, M., 2000. Numerical simulation of breakup of a viscous drop in simple shear flow through a volume-of-fluid method. Phys. Fluids 12, 269–282.

Liu, H., Ba, Y., Wu, L., Li, Z., Xi, G., Zhang, Y., 2018. A hybrid lattice Boltzmann and finite difference method for droplet dynamics with insoluble surfactants. J. Fluid Mech. 837, 381–412.
Liu, H., Zhang, Y., 2010. Phase-field modeling droplet dynamics with soluble surfactants. J. Comput. Phys. 229 (24), 9166–9187.
Mukherjee, S., Berghout, P., Van den Akker, H.E.A., 2019a. A lattice Boltzmann approach to surfactant-laden emulsions. AIChE J. 65 (2), 811–828.
Mukherjee, S., Safdari, A., Shardt, O., Kenjereš, S., Van den Akker, H.E., 2019b. Droplet-turbulence interactions and quasi-equilibrium dynamics in turbulent emulsions. J. Fluid Mech. 878, 221–276.
Pan, K.-L., Tseng, Y.-H., Chen, J.-C., Huang, K.-L., Wang, C.-H., Lai, M.-C., 2016. Controlling droplet bouncing and coalescence with surfactant. J. Fluid Mech. 799, 603–636.
Pozrikidis, C., 2012. Stability of sessile and pendant liquid drops. J. Engrg. Math. 72, 1–20.
Renardy, Y.Y., Renardy, M., Cristini, V., 2002. A new volume-of-fluid formulation for surfactants and simulations of drop deformation under shear at a low viscosity ratio. Eur. J. Mech. - B 21, 49–59.
Shan, X., Chen, H., 1993. Lattice Boltzmann model for simulating flows with multi phases and components. Phys. Rev. E 47 (3), 1815–1819.
Shan, X., Doolen, G.D., 1995. Multicomponent lattice-Boltzmann model with interparticle interaction. J. Stat. Phys. 81, 379–393.
Shang, X., Luo, Z., Bai, B., Hu, G., 2023. A front-tracking method for simulating interfacial flows with particles and soluble surfactants. J. Comput. Phys. 493, 112476.
Shardt, O., Derksen, J., Mitra, S.K., 2014. Simulations of Janus droplets at equilibrium and in shear. Phys. Fluids 26 (1), 012104.
Shi, Y., Tang, G.H., Cheng, L.H., Shuang, H.Q., 2019. An improved phase-field-based lattice Boltzmann model for droplet dynamics with soluble surfactant. Comput. Fluids 179, 508–520.
Skartlien, R., Furtado, K., Sollum, E., Meakin, P., Kralova, I., 2011. Lattice–Boltzmann simulations of dynamic interfacial tension due to soluble amphiphilic surfactant. Phys. A 390 (12), 2291–2302.
Soligo, G., Roccon, A., Soldati, A., 2019. Coalescence of surfactant-laden drops by phase field method. J. Comput. Phys. 376, 1292–1311.
Sui, Y., 2014. Moving towards the cold region or the hot region? Thermocapillary migration of a droplet attached on a horizontal substrate. Phys. Fluids 26 (9), 092102.
Van den Akker, H.E., 2018. Lattice Boltzmann simulations for multi-scale chemical engineering. Curr. Opin. Chem. Eng. 21, 67–75.
Van den Akker, H., Donkers, R., Zachariah, G., Shardt, O., 2021. On using variable molecular masses in multicomponent lattice Boltzmann simulations. J. Comput. Sci. 54, 101432.
Van Der Sman, R.G.M., Meinders, M.B.J., 2016. Analysis of improved lattice Boltzmann phase field method for soluble surfactants. Comput. Phys. Comm. 199, 12–21.
Van der Sman, R.G.M., Van der Graaf, S., 2006. Diffuse interface model of surfactant adsorption onto flat and droplet interfaces. Rheol. Acta 46 (1), 3–11.
Van der Sman, R.G.M., Van der Graaf, S., 2008. Emulsion droplet deformation and breakup with lattice Boltzmann model. Comput. Phys. Comm. 178 (7), 492–504.
van Konynenburg, P.H., Scott, R.L., 1980. Critical lines and phase equilibria in binary van der Waals mixtures. Philos. Trans. R. Soc. A 298 (1442), 495–540.
Xu, J.-J., Li, Z., Lowengrub, J., Zhao, H., 2006. A level-set method for interfacial flows with surfactant. J. Comput. Phys. 212 (2), 590–616.
Yuan, P., Schaefer, L., 2006. Equations of state in a lattice Boltzmann model. Phys. Fluids 18 (4), 042101.
Yun, A., Li, Y., Kim, J., 2014. A new phase-field model for a water-oil-surfactant system. Appl. Math. Comput. 229, 422–432.
Zarghami, A., Looije, N., Van den Akker, H.E.A., 2015. Assessment of interaction potential in simulating nonisothermal multiphase systems by means of lattice Boltzmann modeling. Phys. Rev. E 92 (2), 023307.
Zhang, S.-T., Hu, Y., Li, Q., Li, D.-C., He, Q., Niu, X.-D., 2024. A second-order phase field-lattice Boltzmann model with equation of state inputting for two-phase flow containing soluble surfactants. Phys. Fluid 36, 022104.
Zhang, J., Shu, S., Guan, X., Yang, N., 2021. Regime mapping of multiple breakup of droplets in shear flow by phase-field lattice Boltzmann simulation. Chem. Eng. Sci. 240, 116673.
Zhou, W., Xing, Y., Liu, X., Yan, Y., 2023. Modeling of droplet dynamics with soluble surfactant by multi-relaxation-time phase-field lattice Boltzmann method. Phys. Fluids 35, 012109.
Zong, Y., Zhang, C., Liang, H., Wang, L., Xu, J., 2020. Modeling surfactant-laden droplet dynamics by lattice Boltzmann method. Phys. Fluids 32, 122105.